JOURNAL OF MATERIALS SCIENCE 31 (1996) 3971–3981

# On the effects of second phase distribution on the fracture behaviour of two superplastic aluminium alloys

K. A. PADMANABHAN
*Department of Metallurgical Engineering, Indian Institute of Technology, Madras 600 036, India*

O. ENGLER, K. LÜCKE
*Institut für Metallkunde und Metallphysik, RWTH Aachen, D-52056 Aachen, Germany*

The significant scatter observed in the elongation to fracture of specimens taken from a single, industrially processed sheet for two Al alloys has been traced to changes in the value of the strain rate sensitivity index ($m$) and also to the specimen to specimen variation in the concentration and distribution of second phase particles/inclusions. It is shown that these three variables of $m$, second phase particle content and distribution affect the width of tear ridges, the size of clusters of grains that pull out as a whole during fracture, their connectivity and the extent to which cavitation can be suffered before final fracture. The consequences of these effects for specimen ductility are discussed.

## 1. Introduction

The cavitation behaviour of superplastic alloys is a well reviewed area [1–12]. The process is the result of a mismatch between grain boundary sliding and its accommodation processes. In quasi-single phase materials, cavity nucleation is at grain boundary particles. In microduplex alloys free from boundary particles, cavities nucleate at grain boundary obstacles, e.g., triple point junctions, grain boundary ledges, intersections of cooperatively slid boundaries. In both types of alloys cavity growth is dominated by matrix plastic flow. Local tearing by plastic deformation that connects different crack paths is present during crack growth. Coalescence and interlinkage of cavities can lead to the formation of large cavities, significantly alter the cavity growth rate and adversely affect the post-forming properties. Under optimal conditions of superplastic flow, final fracture is intercrystalline in appearance. Sometimes, for unknown reasons, cavitation leads to grain boundary cracking.

The roles of impurity levels and pre-existing defects as well as the mechanisms and the kinetics of cavity nucleation are not clear. The influence of microstructure and deformation conditions, however, are reasonably well understood. Continuous cavity nucleation may be present when grain growth is significant, e.g. in Al alloys.

A high value of $m$ (strain-rate sensitivity index) confers a high necking resistance on intercavity ligaments and permits a high volume fraction of cavities to develop before fracture. But $m$ is a *macroscopic* property that depends in a complex way on the microstructural and experimental variables.

Ductility is also affected by the density and distribution of second phase particles/inclusions [13, 14]. Cavitation is less when the dispersoids are small and uniformly distributed. Sometimes superplastic elongations are "highly reproducible" [15, 16] but, in general, there is considerable scatter in plots of $m$ versus elongation at fracture [17–19]. This could be due to the non-random distribution of cavity nucleating sites in different specimens and this aspect has not so far been studied in detail. The present investigation attempts to correct this omission.

## 2. Experimental procedure

The procedures for tensile testing, estimating the mechanical properties and correlating them with the texture changes accompanying superplastic flow are described elsewhere [20, 21]. The alloys used for the present study were two industrially processed superplastic alloys (SUPRAL 100 and an Al–Ca–Zn alloy); the compositions of the two alloys are given in Table I. For both alloys, all specimens were cut from a single sheet. It was felt that a study of this kind would be useful as these alloy sheets represent the maximum consistency obtainable in current industrial practice. The fractured specimens of the alloys [20, 21] were subjected to energy dispersive X-ray analysis and scanning electron microscopy. For these investigations, a Jeol 35CF scanning electron microscope was used.

0022–2461 

TABLE I Compositions (wt%) of the alloys:
(a) SUPRAL 100 (Al–Cu–Zr alloy) – Alloy A

| Cu | Zr | Fe | Si | Ni | Mg | Mn | Zn | Ti | Ga | B | Al |
|---|---|---|---|---|---|---|---|---|---|---|---|
| 6.50 | 0.40 | 0.15 | 0.074 | 0.072 | 0.036 | 0.028 | 0.019 | 0.005 | 55 ppm | 7 ppm | Balance |

(b) Al–Ca–Zn alloy – Alloy B

| Ca | Zn | Fe | Si | Mg | Al |
|---|---|---|---|---|---|
| 4.87 | 4.64 | 0.13 | 0.09 | 0.01 | Balance |

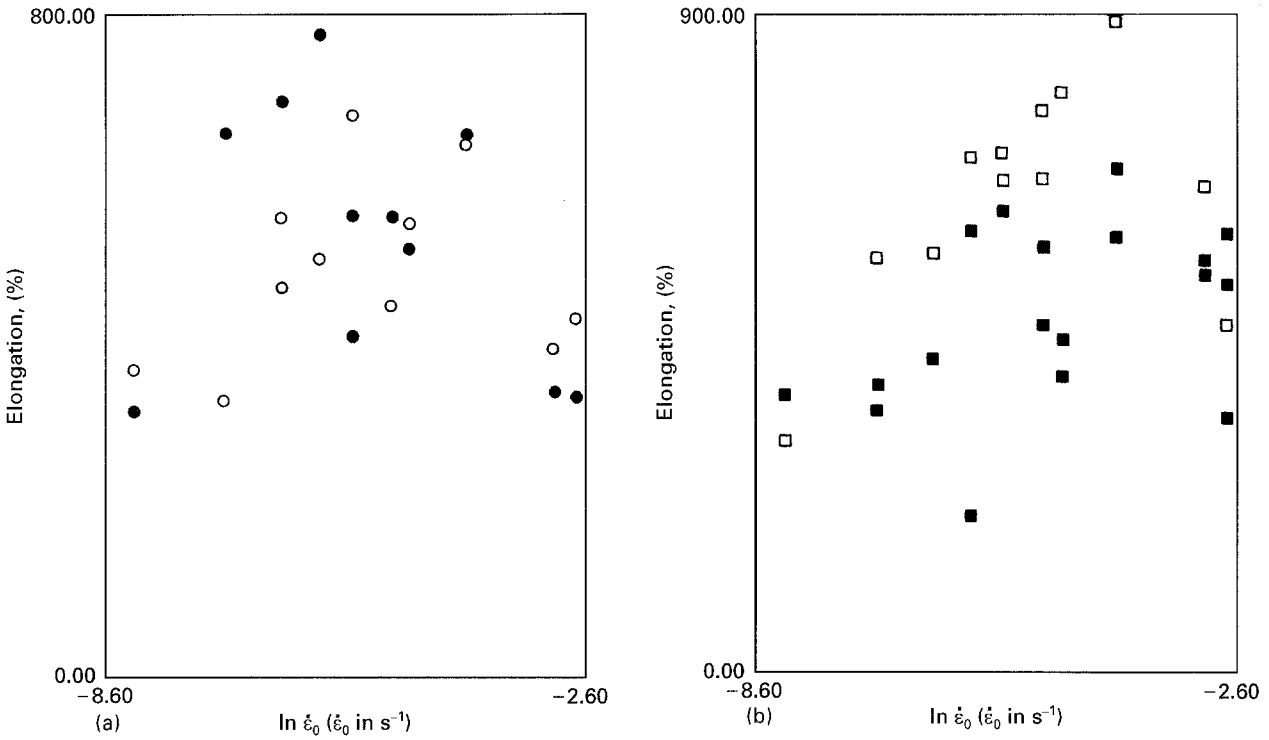


*Figure 1* Elongation at fracture $-\ln(\dot{\varepsilon}_0)$ relationship in case of (a) alloy A (730 K), and (b) alloy B (825 K). The suffix L denotes that the specimen axis was parallel to the sheet rolling direction and the suffix T indicates that the transverse direction of the sheet was parallel to the tensile axis. The symbols represent data taken for (○) $A_L$, (●) $A_T$, (□) $B_L$ and (■) $B_T$.

## 3. Results and discussion

### 3.1. Tensile tests

Supral 100 (alloy A*) had an as-received two dimensional equiaxed average grain size of $2.2 \pm 0.2$ μm, with a few grains being as large as 5.0 μm. In room temperature (20 °C) constant crosshead speed tests at an initial strain rate ($\dot{\varepsilon}_0$) of $1.7 \times 10^{-3}\ s^{-1}$, an elongation at fracture of 8% was obtained in both the sheet rolling and the transverse directions.

The Al–Ca–Zn alloy (Alloy B*) had an as-received two dimensional equiaxed average grain size of $1.7 \pm 0.4$ μm. Rarely particles as large as 4.3 μm with an aspect ratio of about 2.4 were also seen. In this material the room temperature elongation at fracture in both the sheet rolling and the transverse directions was 6%. Fig. 1 (a and b) displays the elongation at fracture $-\ln(\dot{\varepsilon}_0)$ relationship for both the alloys at their respective optimal temperature of superplastic flow, i.e. at 730 K (457 °C; alloy A) and 825 K (552 °C; alloy B). The scatter was large, except for Alloy B tested in the sheet rolling direction ($B_L$).

### 3.2. Energy dispersive X-ray analysis

It is known that in Al–Cu–Zr alloys, $ZrAl_3$ and $CuAl_2$ particles cause cavitation while in dilute Al–Cu alloys the $CuAl_2$ particles are responsible for the cavitation [2, 22]. No such information is available with regard to the Al–Ca–Zn alloy. In the present study, the chemical composition of a multitude of precipitates was analysed by energy dispersive X-ray analysis in a scanning electron microscope (Fig. 2). As most precipitates were too small for quantitative analysis (i.e. <1 μm), only qualitative information about the composition could be obtained. In particular, the amount of Al being the main element in the matrix can be strongly misleading in the plots.

In Alloy A, pure $CuAl_2$ and also a variant containing a small amount of Fe and traces of Zr were seen (Fig. 2 (a and b)). No $ZrAl_3$ precipitates could be identified, since they are only a few tens of nanometers in size and thus can only be revealed by high resolution transmission electron microscopy [19].

* Alloys A and B are referred to as alloys B and C respectively in Refs. [20, 21].

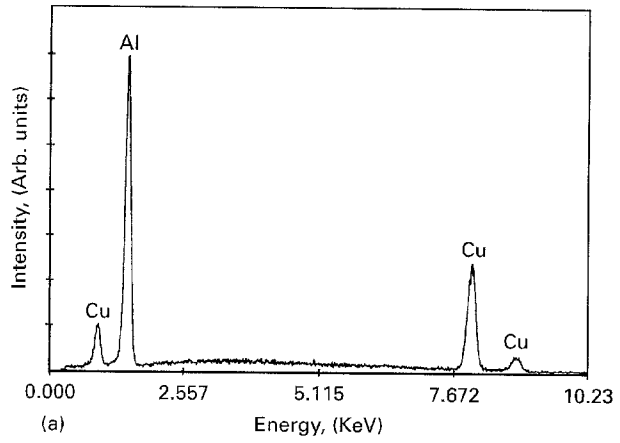


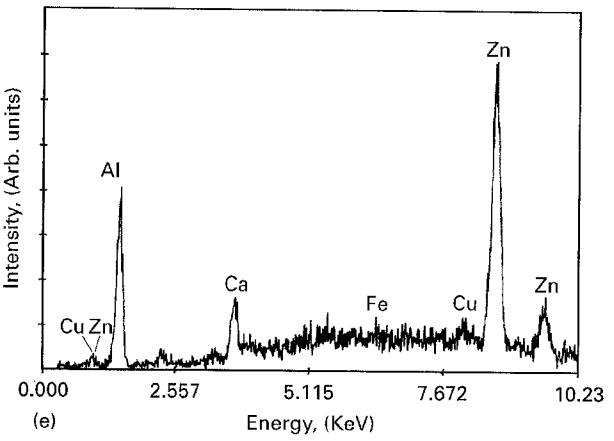


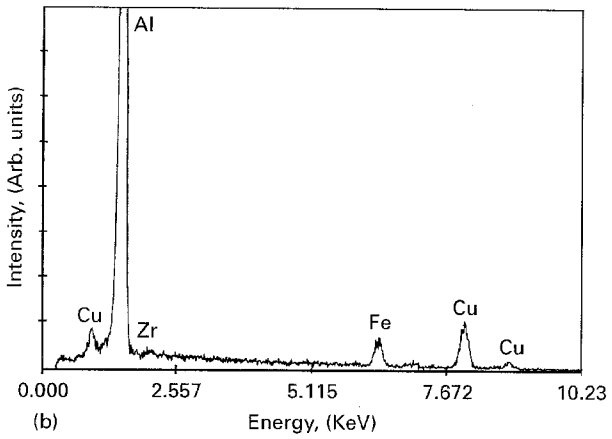


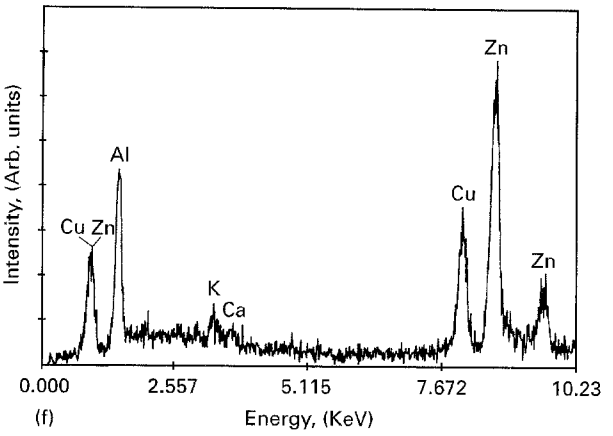


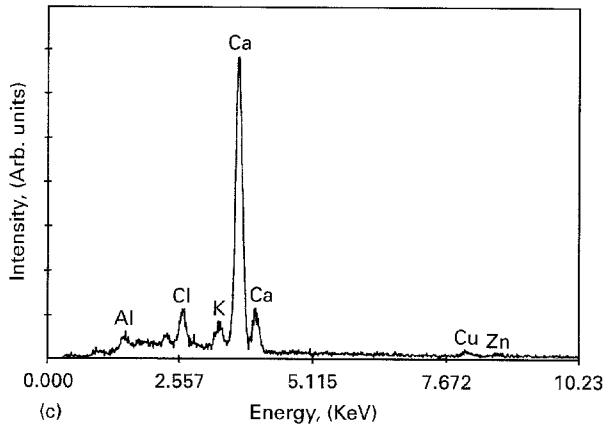


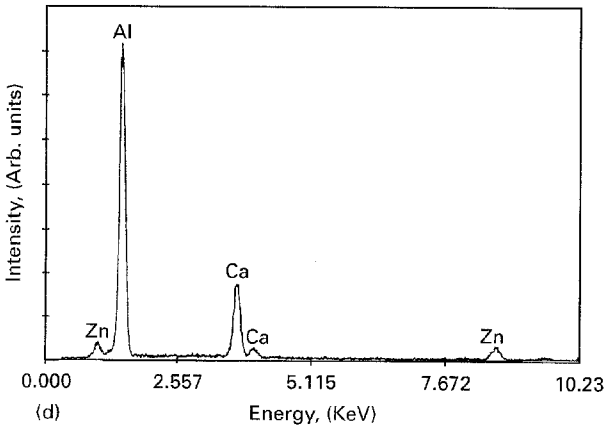


*Figure 2* Energy dispersive X-ray analysis of precipitates present in alloys A (a, b) and B (c–f): (a) pure $CuAl_2$; (b) $CuAl_2$ containing a small amount of Fe and traces of Zr; (c) a Ca-rich precipitate containing small amounts of other elements; (d) an Al-rich precipitate containing Ca and a small amount of Zn; (e) a Zn-rich precipitate with Al as the other important element but also containing small amounts of Ca and other elements; (f) a Zn-rich precipitate with Al and Cu as the other important elements, but also containing small amounts of Ca.

In Alloy B, four types of precipitates were present: (i) a Ca-rich precipitate that contained small amounts of Al, Cu, and Zn (Fig. 2c), (ii) an Al-rich precipitate containing a significant level of Ca and a small amount of Zn (Fig. 2d), (iii) two variants of a Zn-rich precipitate: one with Al as the other important element but also containing small amounts of Ca and Fe and traces of Cu (Fig. 2e); and secondly a variant of this precipitate in which the level of Cu was more and the absence of Fe was noted (Fig. 2f).

The distribution and density of these precipitates/second phase particles varied from one specimen to the next and in the next section this is suggested to be the reason for the scatter in the ductility data.

## 3.3. Scanning electron microscopy

The results were similar for both alloys and so they are discussed together. Consistent with the very limited elongations observed, room temperature fracture was non-uniform and the dimples were very shallow (Fig. 3). Under conditions of superplastic flow, the following correlations between the features of fracture and the elongation at failure could be established.

(i) As *tearing* connects independent crack paths by plastic deformation, the width of the tear ridges

decreased with increasing boundary sliding contribution/ductility, as is shown in Fig. 4 (a and b). In Fig. 4b sliding was more uniform, cavitation was dispersed at more boundaries (both of which depended on the distribution of the second phase(s) in the specimen) and $m$ was greater [20] than in Fig. 4a. Thus the observed difference in ductility was a combined effect of the changes in the distribution of the second phases and the $m$ value that depended on both the microstructure and the strain rate of deformation.

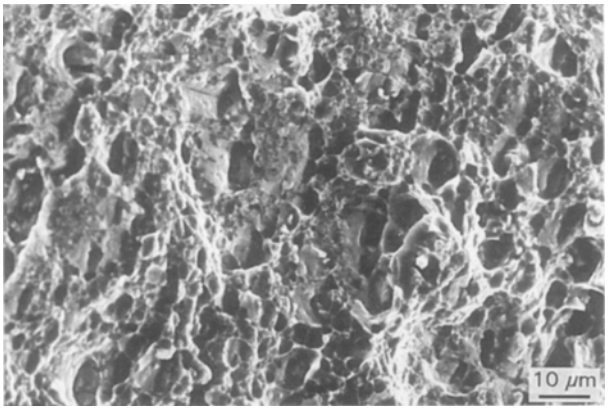


*Figure 3* The fracture surface of a specimen of alloy $A_T$ tested at room temperature; $\dot{\varepsilon}_0 = 1.7 \times 10^{-3}\,s^{-1}$; elongation at fracture 8%.

(ii) *The size of the clusters of grains that pulled out as a whole at fracture* depended on the distribution of the second phase(s). When this size was large (due to the pattern of distribution of the second phase particles), a significant number of boundaries were bypassed in the sliding process and this led to a drastic decrease in ductility (Fig. 5 (a–c)). In Fig. 5a the cluster size was significantly larger than in Fig. 5 (b and c) and $m$ was also smaller [20].

(iii) If the crack paths included many *triple point junctions* (regions of high stress concentration), due say to the nature of the interfaces and/or chemical segregation, then the ductility decreased considerably (Fig. 6).

(iv) *Precipitates/second phase particles* were present on the *fracture surfaces* even when the elongation was maximum (Fig. 7 (a and b)). It was clear that particle/matrix decohesion was a major cause of cavitation and fracture.

(v) In Alloy A, even though $m$ was greater at $\dot{\varepsilon}_0 = 6.6 \times 10^{-3}\,s^{-1}$ than at $\dot{\varepsilon}_0 = 1.7 \times 10^{-2}\,s^{-1}$ [20], the elongation was larger at the latter strain rate (Fig. 8 (a and b)). In Fig. 8a the distribution of the second phase particles gave rise to contiguous clusters of grains that were interlinked by cavitation. In this process many boundaries were bypassed by the growing cracks, while at the same time large areas were rendered weak. In such a situation the ductility was understandably lower. A similar observation could

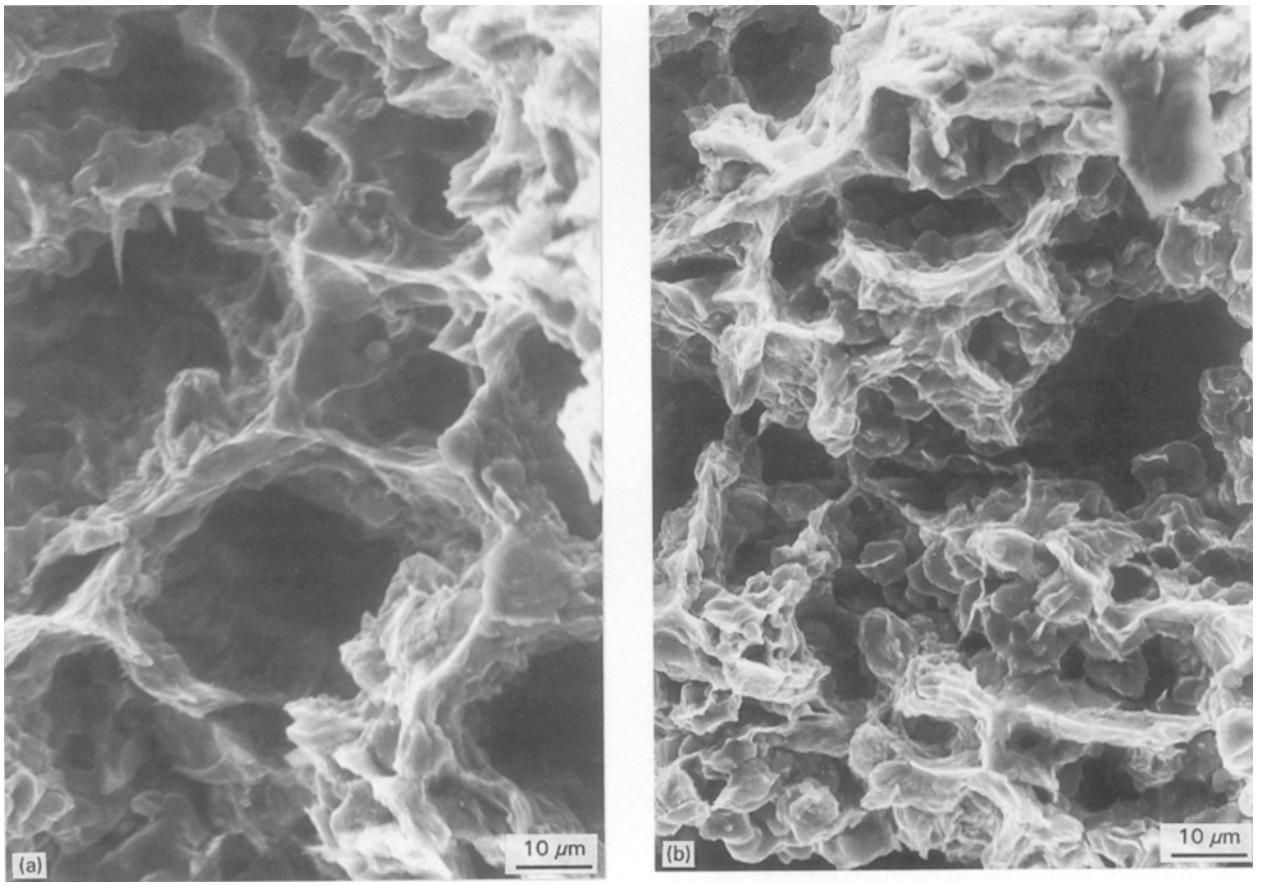


*Figure 4* When sliding and cavitation were more uniform, the width of the tear ridges at the boundaries decreased and the ductility increased; $A_L$ specimens; (a) elongated by 371% at fracture at $\dot{\varepsilon}_0 = 2.7 \times 10^{-4}\,s^{-1}$; (b) elongated by 680% at fracture at $\dot{\varepsilon}_0 = 4.0 \times 10^{-3}\,s^{-1}$.

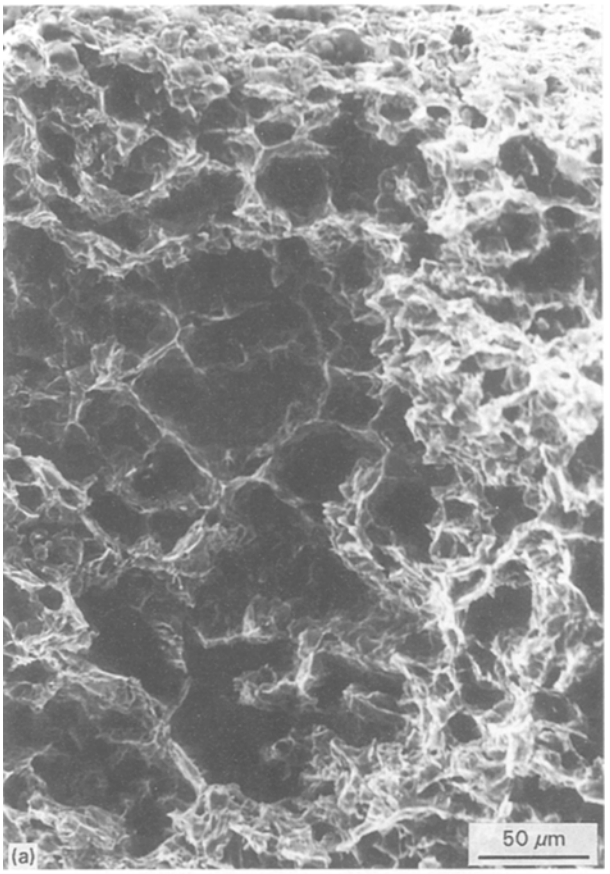


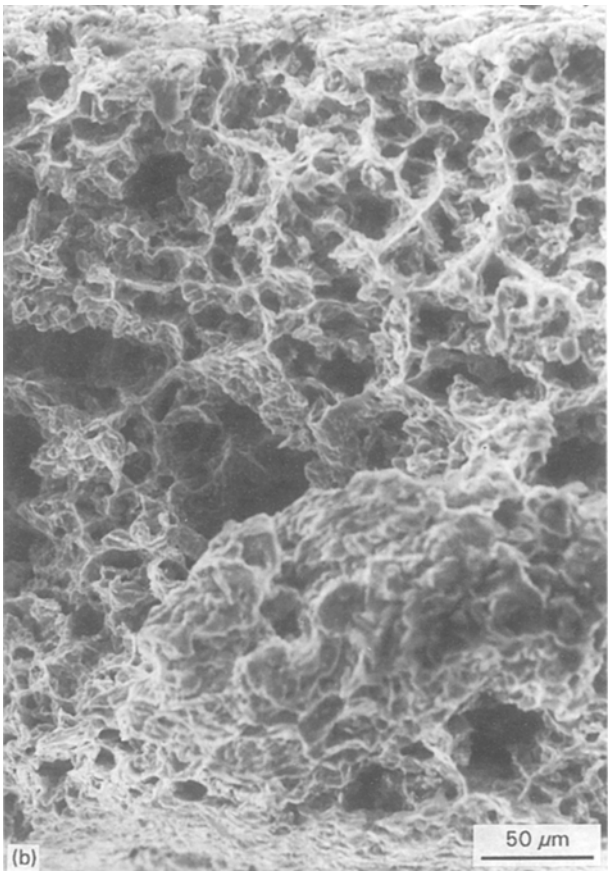


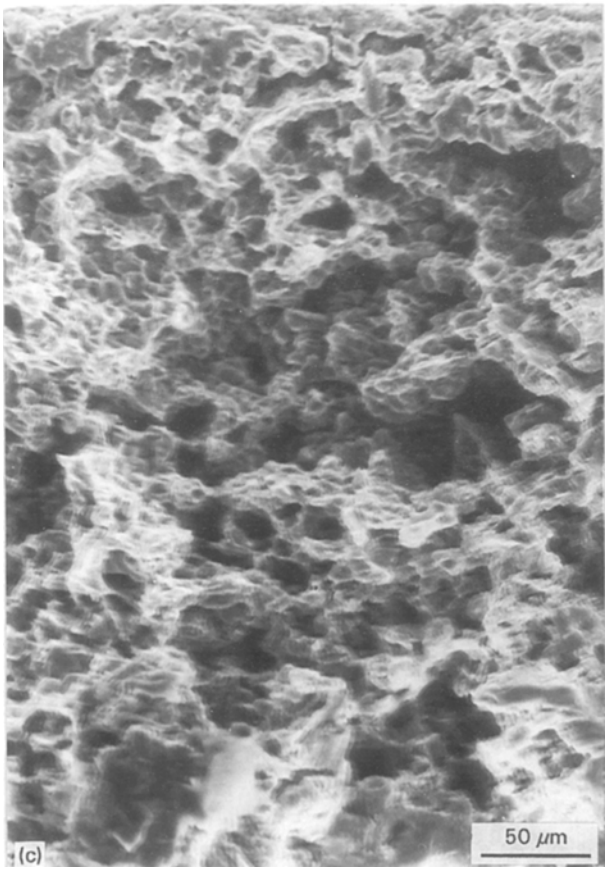


*Figure 5* The ductility and the size of the clusters of grains that pulled out as a whole were inversely related; $A_L$ specimens; (a) elongated by 371% at fracture at $\dot{\varepsilon}_0 = 2.7 \times 10^{-4}\,s^{-1}$; (b) elongated by 680% at fracture at $\dot{\varepsilon}_0 = 4.0 \times 10^{-3}\,s^{-1}$; (c) an $A_T$ specimen elongated by 781% at fracture at $\dot{\varepsilon}_0 = 2.7 \times 10^{-3}\,s^{-1}$.

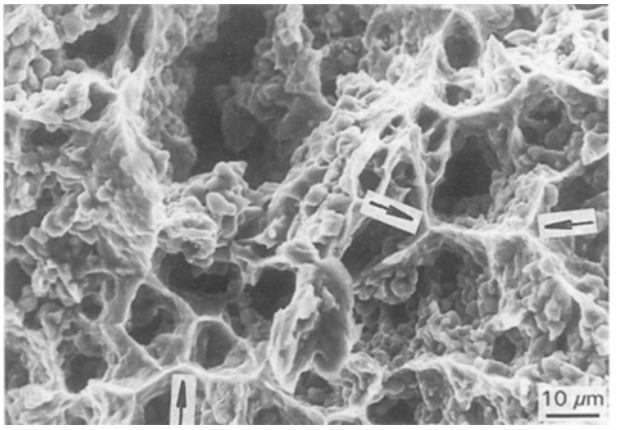


*Figure 6* Clusters of grains pulling out along networks that included triple point junctions (arrowed); an $A_L$ specimen elongated by 400% at fracture at $\dot{\varepsilon}_0 = 5.0 \times 10^{-2}\,s^{-1}$.

also be made with Alloy $B_T$, see Fig. 8 (c and d) (In Fig. 8c the clusters of grains that pulled out as a whole were larger and often contiguous).

(vi) Two specimens of Alloy $B_L$ were pulled to failure at the same initial strain rate of $\dot{\varepsilon}_0 = 1.7 \times 10^{-3}\,s^{-1}$ (Figs 9 (a and b)). In Fig. 9a the concentration of particles in the fracture zone was more than in Fig. 9b and understandably the elongation was less in the former case.

(vii) On the fracture surface in a region that was in the specimen interior until fracture, even after extreme elongation, the grain shape was rather similar to the starting shape (Fig. 10). This was clear evidence for the importance of boundary deformation processes throughout superplastic flow.

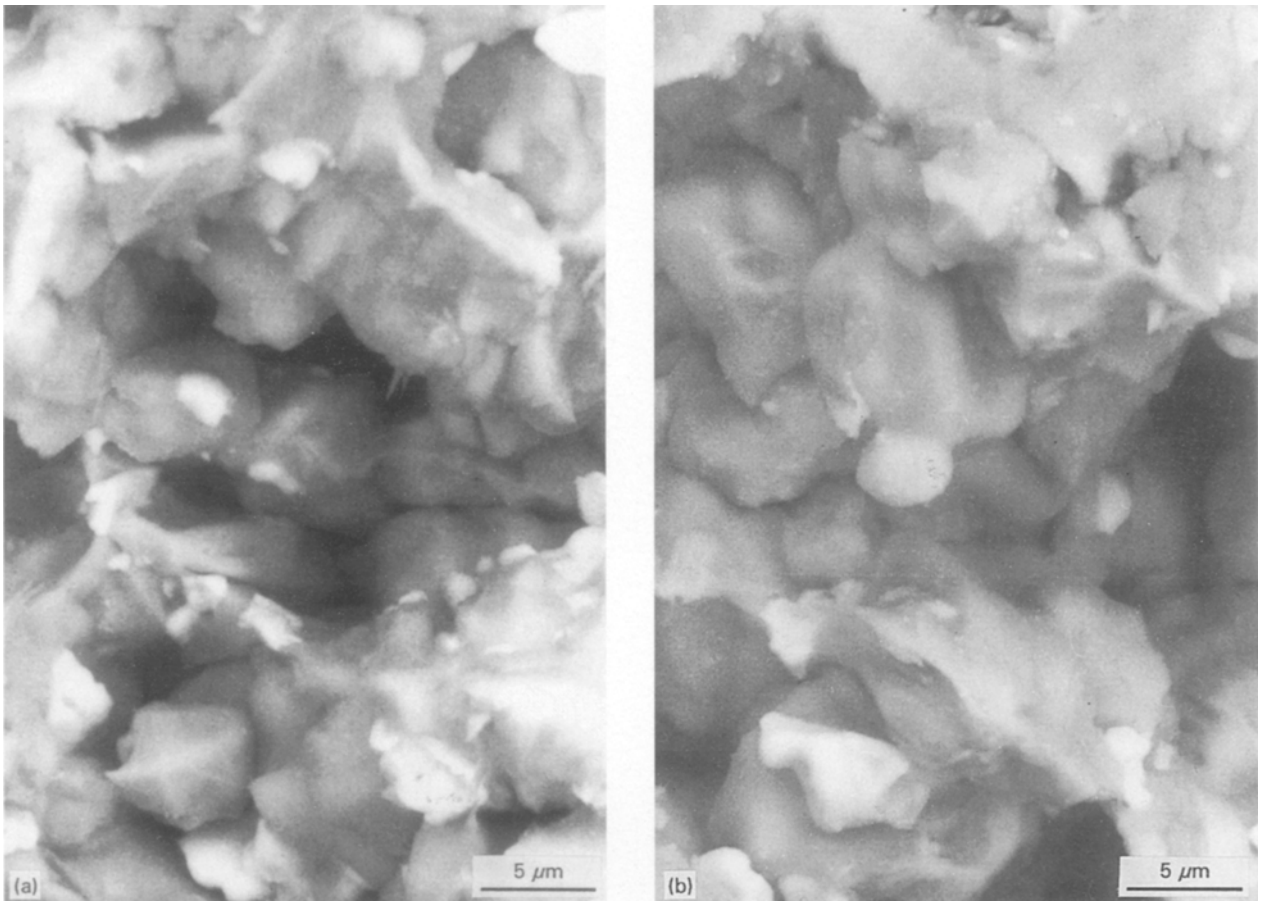


*Figure 7* Second phase particles are present on the fracture surface even when the elongation at fracture was maximum; (a) an $A_L$ specimen elongated by 680% at fracture at $\dot{\varepsilon}_0 = 4.0 \times 10^{-3}\,s^{-1}$; (b) an $A_T$ specimen elongated by 781% at fracture at $\dot{\varepsilon}_0 = 2.7 \times 10^{-3}\,s^{-1}$ (pictures taken using back-scattered electrons).

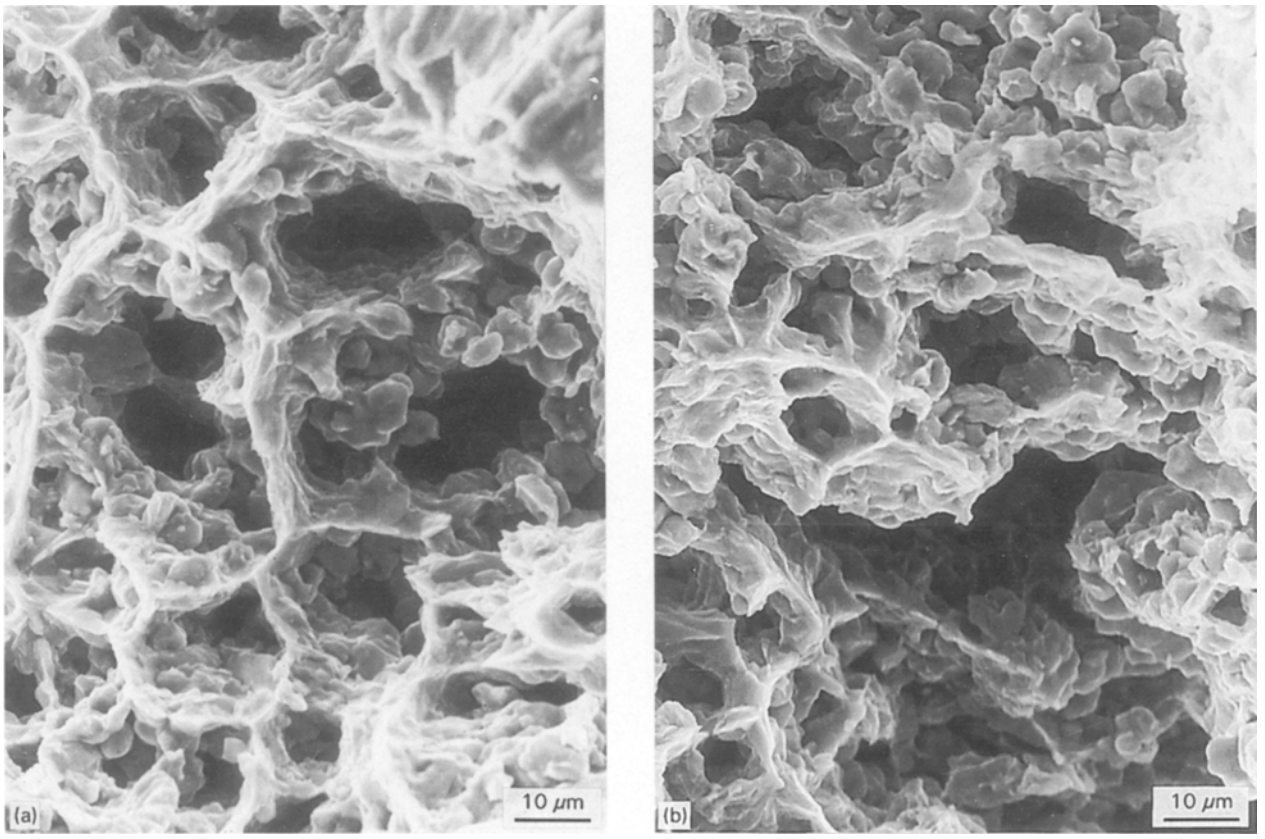


*Figure 8* A deleterious distribution of second phase particles/inclusions leading to ductility loss even when $m$ had increased: (a) and (b) $A_L$ specimens elongated by 449% (higher $m$) and 645% at fracture respectively at $\dot{\varepsilon}_0 = 6.6 \times 10^{-3}\,s^{-1}$ and $1.7 \times 10^{-2}\,s^{-1}$; (c) and (d) $B_T$ specimens elongated by 407% (higher $m$) and 597% at fracture respectively at $\dot{\varepsilon}_0 = 8.3 \times 10^{-3}\,s^{-1}$ and $1.7 \times 10^{-2}\,s^{-1}$.

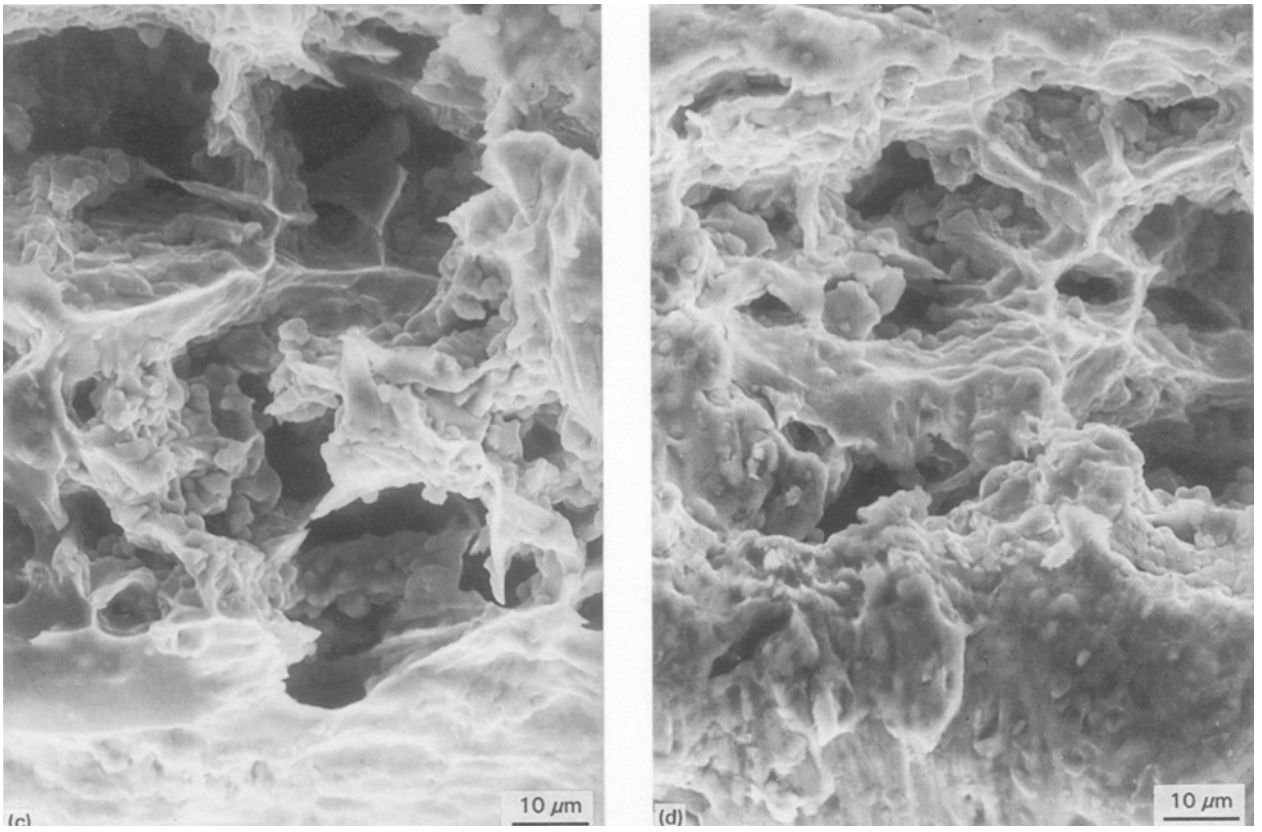


*Figure 8* (Continued).

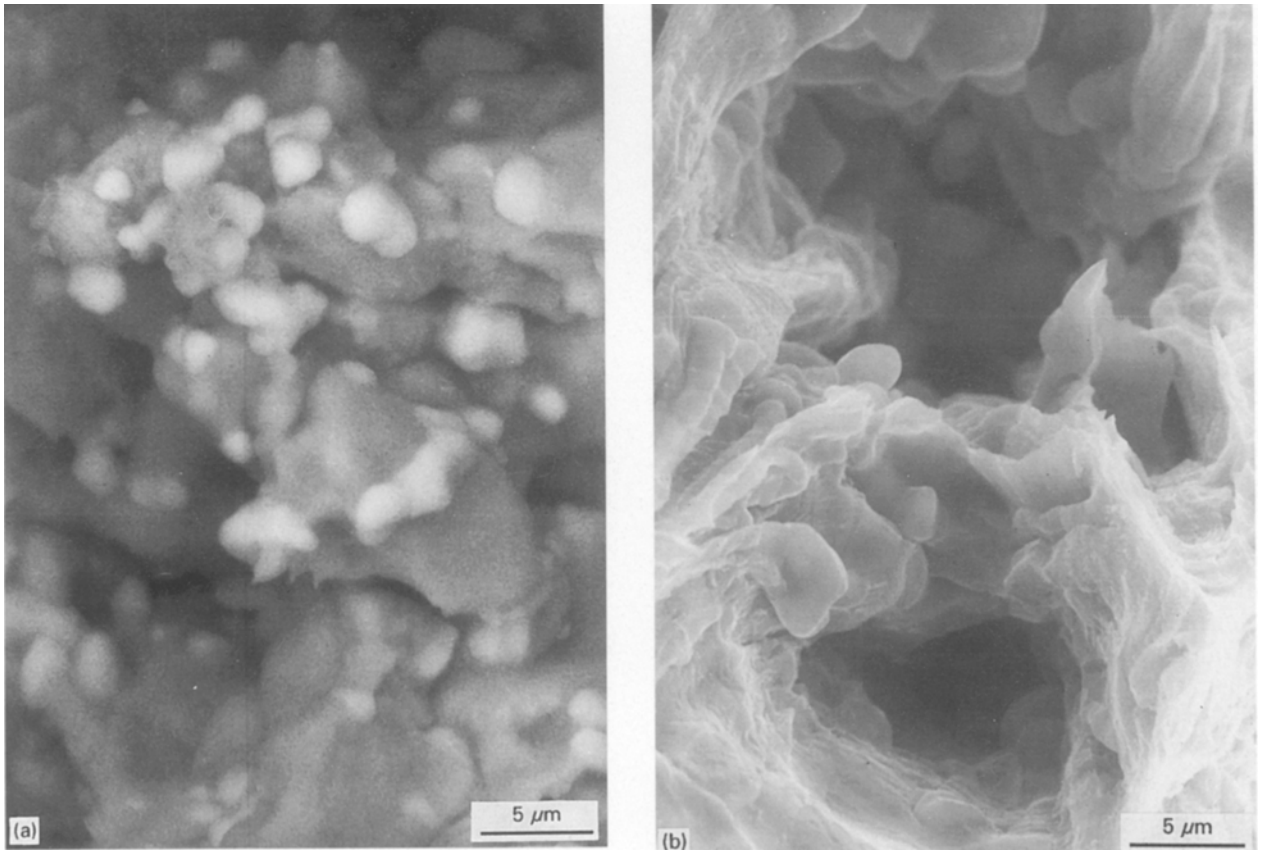


*Figure 9* The ductility decreased when the concentration of second phase particles/inclusions in the fracture zone was greater. $B_L$ specimens (a) elongated by 572% at fracture at $\dot{\varepsilon}_0 = 1.7 \times 10^{-3}\,s^{-1}$ (the large number of precipitate particles on the fracture surface was revealed using back-scattered electrons); (b) elongated by 658% at fracture at the same $\dot{\varepsilon}_0$ (note the much cleaner fracture surface).

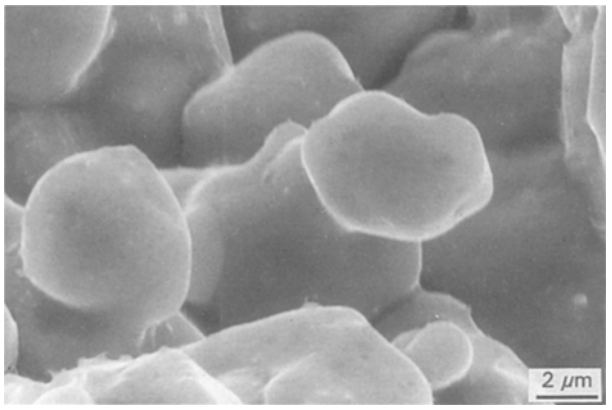


*Figure 10* Equiaxed grain shape found at high magnification in the interior of a specimen elongated by 781% at fracture; $\dot{\varepsilon}_0 = 2.7 \times 10^{-3}\,s^{-1}$; an $A_T$ specimen.

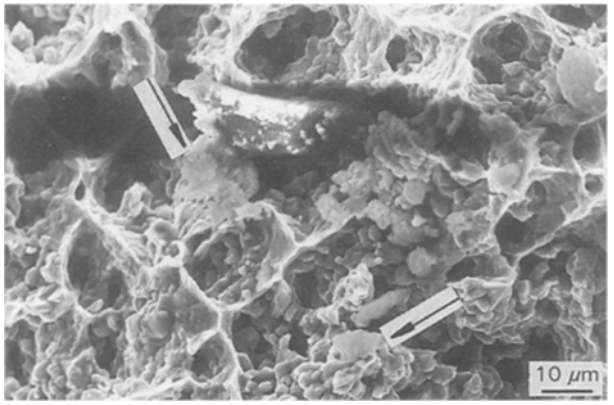


*Figure 11* A fractograph displaying many deleterious features due to high concentration of second phase particles in the fracture zone. An $A_T$ specimen tested at $\dot{\varepsilon}_0 = 6.6 \times 10^{-2}\,s^{-1}$ (see text).

(viii) When the concentration of the second phase particles in the zone of fracture was high, a steep drop in ductility resulted, as is shown in Fig. 11. The ductility decreased to 343% from 660% when the initial strain rate was reduced only by a factor of 4. In Fig. 11 the following undesirable features are present on the fracture surface: a number of second phase particles, two long horizontal cracks, pulling out of contiguous clusters of grains of fairly large sizes, some featureless regions (arrowed), which could be indicative of fracture of second phase particles. Fig. 11 corresponded to the highest strain rate employed in the present investigation and fell in the region of transition from region II(b) to region III of superplastic flow [18, 19].

(ix) On the lateral surfaces of specimens adjacent to the region of fracture, the following features were noticed.

(a) Surface delamination/void formation was present on the lateral surface. The density of voids had increased near the fracture tip (Fig. 12).

(b) Necking was more severe in alloy B than in Alloy A. Thus, in the former alloy the surface grains in the severely necked region have elongated significantly even at the lowest strain rate ($\dot{\varepsilon}_0 = 2.7 \times 10^{-4}\,s^{-1}$). The cavities on the lateral surface in the necked region were rounded and separated (Fig. 13a) or elongated with the major axis nearly perpendicular to the stress

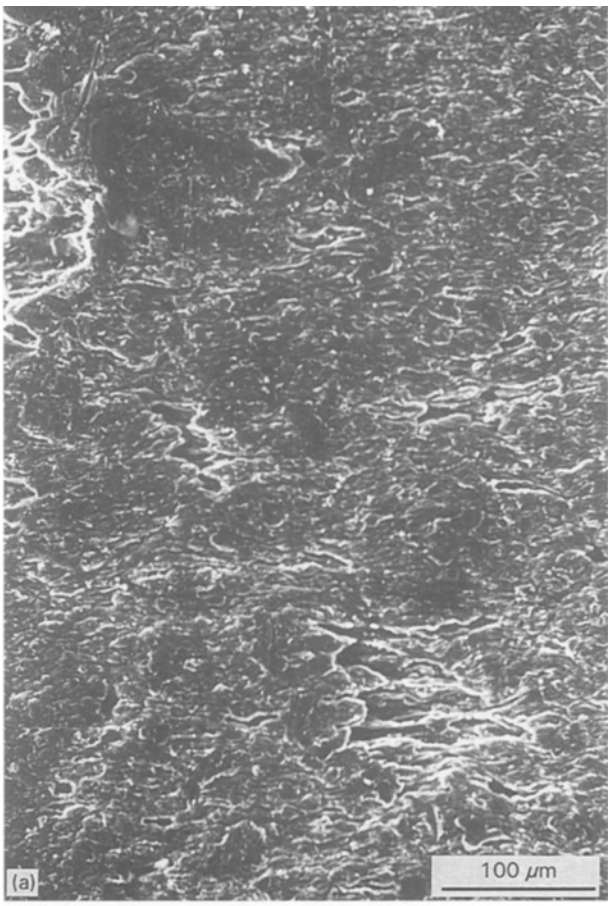


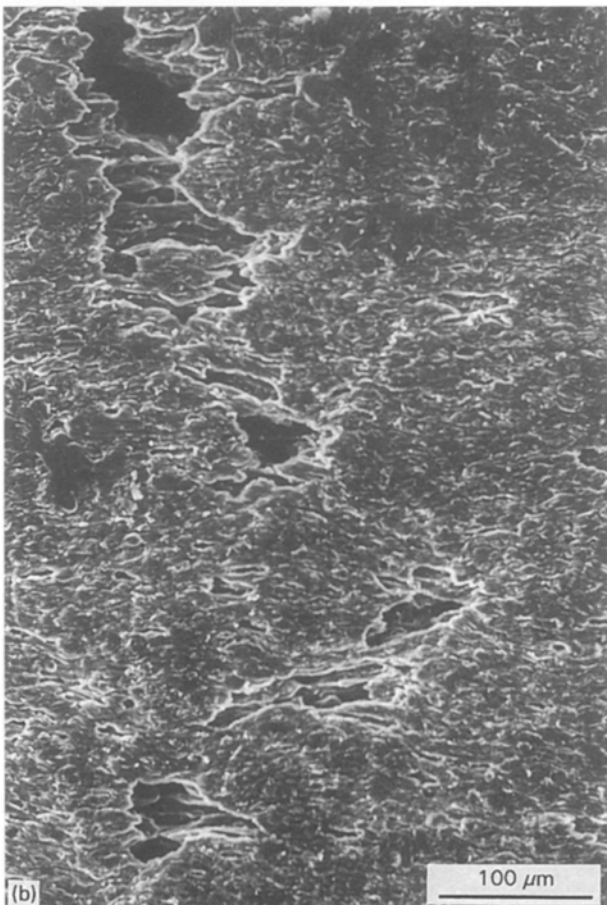


*Figure 12* The few surface voids seen in (a) had increased in density in (b), taken near the fracture tip; 510% elongation at fracture; $\dot{\varepsilon}_0 = 2.7 \times 10^{-3}\,s^{-1}$; an $A_L$ specimen.

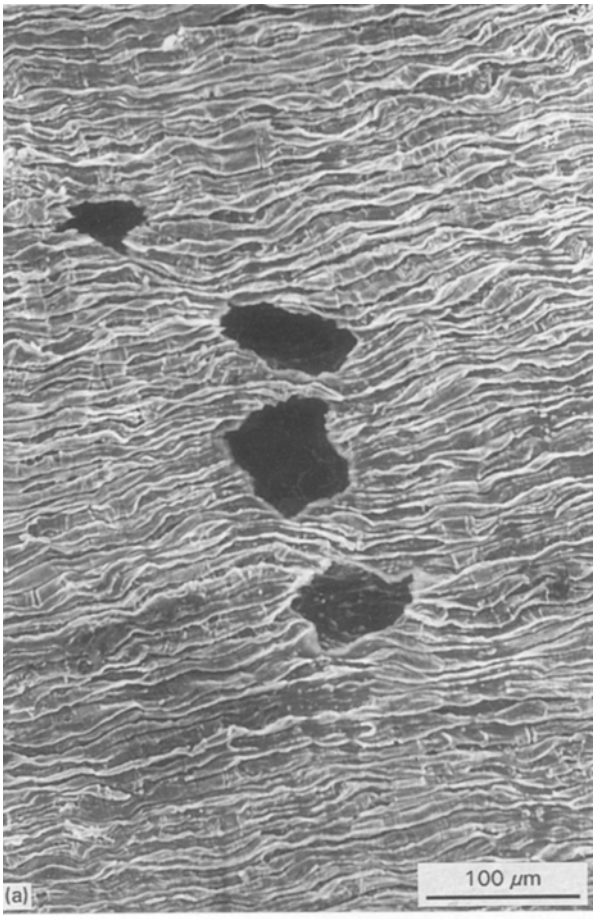



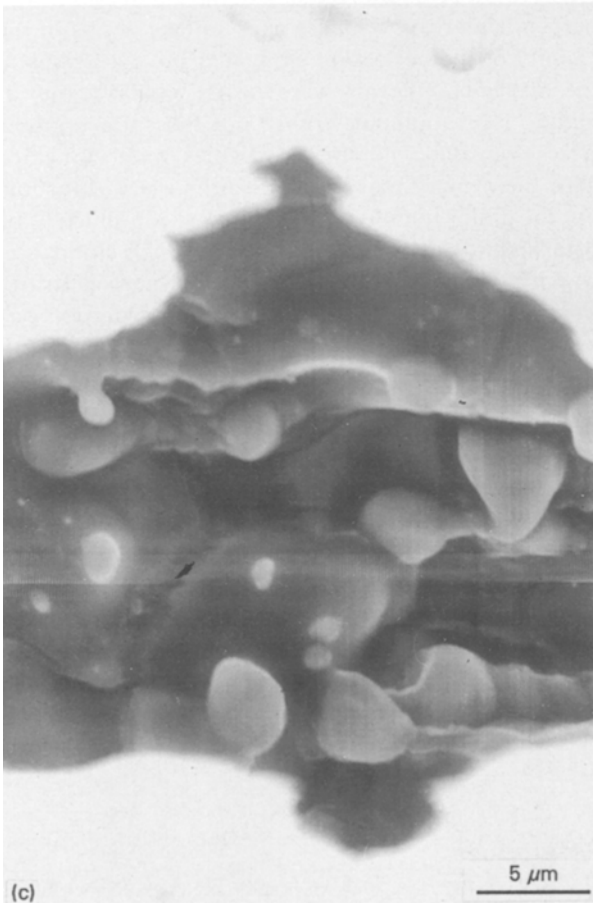


*Figure 13* (a) Grain elongation and the formation of separate rounded cavities in the necked region of a $B_L$ specimen; $\dot{\varepsilon}_0 = 2.7 \times 10^{-4}\,s^{-1}$; elongation at fracture 387%; (b) a $B_T$ specimen tested at the same $\dot{\varepsilon}_0$; an elongated cavity, with its major axis nearly perpendicular to the stress axis is seen; elongation at fracture 381%. (c) Interior (nearly equiaxed) grains seen through the surface cavity in (b).

axis (Fig. 13b). When the specimen interior was examined through a gap in the lateral surface in the necked region, the grains were seen to be reasonably well rounded (Fig. 13c). This implies that the bulk of the specimen deformed at a strain rate close to the external value but that the surface strain rate (less constraints) was greater. At a higher, more optimal strain rate lateral surface grains in the necked region were also highly elongated and elongated cavities with the major axis parallel to the stress direction were seen (Fig. 14). But, the interior grains were, as before, reasonably well rounded.

(c) In a $B_L$ specimen at the strain rate corresponding to maximum elongation (highest $m$), the surface grains in the severely necked region of the lateral surface would have deformed at a strain rate in region III of superplastic flow. Here, the surface grains were highly elongated and no voiding could be seen on the lateral surface (Fig. 15) which indicated that the contribution from boundary sliding has drastically decreased in this region.

The present study has shown that the density and distribution of the second phase particles/inclusions is far from uniform even in a single industrially

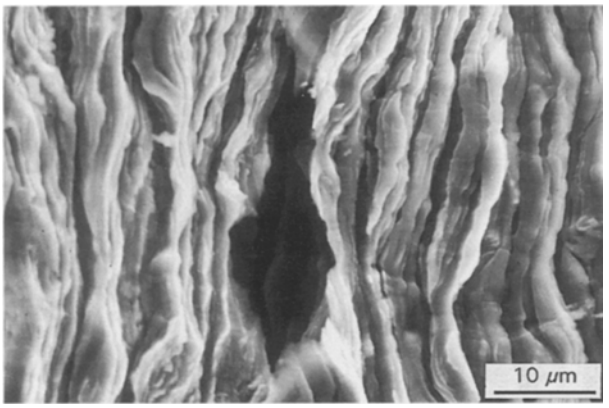


*Figure 14* Severe grain elongation and elongated surface cavity formation in the necked region of a $B_L$ specimen; $\dot{\varepsilon}_0 = 4.0 \times 10^{-3}\,s^{-1}$; elongation at fracture 709%.

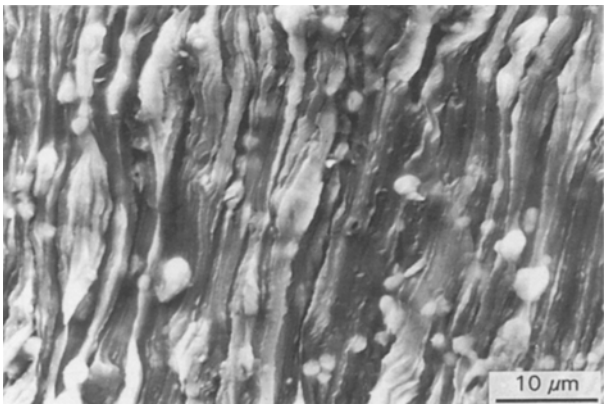


*Figure 15* Highly elongated grains in the severely necked region of a specimen of alloy $B_L$; $\dot{\varepsilon}_0 = 1.7 \times 10^{-2}\,s^{-1}$; elongation at fracture 892% (see text).

processed sheet and that this significantly affects the fracture behaviour. Making this distribution uniform appears to be an interesting challenge to advanced materials technology.

From a fundamental point of view, a study like the present one is useful in understanding "grain boundary character distribution" which in the long run will facilitate the development of theories of cooperative deformation processes [23–26].

## 4. Conclusions

Based on the present fractographic study of two industrially processed alloys – sheets of an Al–Cu–Zr and an Al–Ca–Zn alloy – the following conclusions can be drawn.

1. The significant scatter observed in the ductility of specimens taken from a single sheet should be attributed to specimen to specimen variations in the values of $m$ and to the density and distribution of second phase particles/inclusions.

2. A decrease in the width of the tear ridges (that connect different fracture paths and arise from dislocation processes) leads to an increase in ductility.

3. When the crack paths around clusters of grains that pull out as a whole included many triple point junctions, there is a drastic decrease in ductility.

4. The observation of second phase particles/inclusions on the fracture surface even when the elongation at fracture was maximum, implied that particle/matrix interface decohesion is a major source of cavitation and fracture in the two alloys.

5. The ductility was inversely related to the size of the clusters of grains that pulled out as a whole during fracture since with an increase in cluster size an increasing number of grain boundaries (that display high resistance to internal necking) were bypassed by the fracture processes. For the same reasons, the ductility also decreased sharply when the clusters of grains formed contiguous networks.

6. The ductility decreased significantly if the concentration of second phase particles/inclusions was high in the volume in which the terminal neck and the fracture surfaces were located.

7. Retention of an equiaxed grain shape in the specimen interior following extreme elongation provided evidence for the importance of boundary deformation processes in superplasticity.

8. At the highest strain rate employed in the present tests ($\dot{\varepsilon}_0 = 6.6 \times 10^{-2}\,s^{-1}$) there was some evidence for the fracture of the second phase particles/inclusions.

9. An examination of the lateral side of tested specimens revealed the following: (a) surface cavity formation/delamination of increasing intensity as one approached the fracture tip was observed; (b) at the lowest strain rate ($\dot{\varepsilon}_0 = 2.7 \times 10^{-4}\,s^{-1}$) cavities were either rounded or elongated with the major axis nearly perpendicular to the stress axis, surface grains in the vicinity of the neck were elongated but the grains in the specimen interior were nearly equiaxed; (c) at higher, more optimal strain rates the surface grains were elongated, the surface cavities were elongated with their major axis parallel to the stress direction, but the grains in the specimen interior continued to be equiaxed; (d) at the strain rate for which elongation was maximum, in the necked region surface grains were severely elongated but no surface cavitation was present, both these features indicate that the unconstrained surface region deformed at a strain rate corresponding to region III (while the bulk of the specimen experienced near-optimal superplastic flow).

## Acknowledgements

The Al–Cu–Zr and the Al–Ca–Zn alloys were supplied respectively by Dr. R. Grimes and Dr. D. M. Moore of Alcan. The authors thank Dr. W. G. Burchard for allowing the use of a scanning electron microscope. KAP thanks the Alexander von Humboldt Stiftung, Bonn, for a "Forschungspreis".

## References

1. N. RIDLEY and Z. C. WANG, in Proceedings of Superplasticity in Advanced Materials, Moscow, edited by T. G. Langdon (ICSAM-94), published as *Mater. Sci. Forum* **170–172** (1994) 177.
2. M. J. STOWELL, in "Superplastic Forming of Structural Alloys", edited by N. E. Paton and C. H. Hamilton (TMS-AIME, Warrendale, PA., USA, 1982) p. 321.

3. N. RIDLEY and J. PILLING, in "Superplasticity", edited by B. Baudelet and M. Suery (CNRS, Paris, 1985) paper 8.
4. M. SUERY, *ibid.*, paper 9.
5. A. H. CHOKSHI and A. K. MUKHERJEE, in "Superplasticity and Superplastic Forming", edited by C. H. Hamilton and N. E. Paton (TMS, Warrendale, PA., USA, 1988) p. 149.
6. A. H. CHOKSHI, in "Superplasticity in Advanced Materials" (ICSAM-91), edited by S. Hori, M. Tokizane and N. Furushiro (JSRS, Osaka, Japan, 1991) p. 171.
7. J. PILLING, *ibid.*, p. 181.
8. M. J. STOWELL, in "Deformation of Multi-Phase and Particle Containing Materials" (4th Risø Int. Symp.) edited by J. B. Bilde-Sørensen, N. Hansen, A. Horsewell, T. Leffers and H. Lilholt (Risø National Laboratory, Roskilde, Denmark, 1983) p. 119.
9. B. P. KASHYAP and A. K. MUKHERJEE, *Res. Mechanica* **17** (1986) 293.
10. J. PILLING and N. RIDLEY, *ibid.* **23** (1988) 31.
11. *Idem.*, "Superplasticity in Crystalline Solids", (Institute of Metals, London, 1989).
12. V. N. PEREVEZENTSEV, V. V. RYBIN, and V. N. CHUVIL'DEEV, *Acta Metall. Mater.* **40** (1992) 915.
13. C. H. CACERES and D. S. WILKINSON, in "Superplastic Forming of Structural Alloys", edited by N. E. Paton and C. H. Hamilton (TMS-AIME, Warrendale, PA., USA, 1982) p. 408.
14. P. M. HAZZLEDINE, in "Deformation of Multi-Phase and Particle Containing Materials" (4th Risø Int. Symp.) edited by J. B. Bilde-Sørensen, N. Hansen, A. Horsewell, T. Leffers and H. Lilholt (Risø National Laboratory, Roskilde, Denmark, 1983) p. 27.
15. B. M. WATTS, M. J. STOWELL, B. L. BAIKIE and D. G. E. OWEN, *Metals Sci.* **10** (1976) 189.
16. T. G. LANGDON, in "Superplastic Forming of Structural Alloys", edited by N. E. Paton and C. H. Hamilton (TMS-AIME, Warrendale, PA., USA 1982) p. 30.
17. K. A. PADMANABHAN and K. LÜCKE, *Z. Metallkde.* **77** (1986) 765.
18. J. W. EDINGTON, K. N. MELTON and C. P. CUTLER, *Prog. Mater. Sci.* **21** (1976) 61.
19. K. A. PADMANABHAN and G. J. DAVIES, "Superplasticity" (Springer-Verlag, Berlin, 1980).
20. K. A. PADMANABHAN, J. HIRSCH and K. LÜCKE, *J. Mater. Sci.* **26** (1991) 5301.
21 *Idem., ibid.* **26** (1991) 5309.
22. A. C. F. COCKS and M. F. ASHBY, *Prog. Mater. Sci.* **27** (1982) 189.
23. K. A. PADMANABHAN and J. SCHLIPF, *Mater. Sci. Technol.* (in press).
24. V. V. ASTANIN, S. N. FAIZOVA and K. A. PADMANABHAN, *ibid.* (in press).
25. V. V. ASTANIN, K. A. PADMANABHAN and S. S. BHATTACHARYA, *ibid.* (in press).
26. T. A. VENKATESH, S. S. BHATTACHARYA, K. A. PADMANABHAN and J. SCHLIPF, *ibid.* (in press).

*Received 7 September 1995*
*and accepted 15 January 1996*